Theor Chem Acc (2013) 132:1373
DOI 10.1007/s00214-013-1373-5

REGULAR ARTICLE

Theoretical study on the electronic structure and reactivity of the series of compounds $[Au_3X_3M_2]$, with X = H, F, Cl, Br, I and M = Li, Na, K, Rb, Cs: the quest for novel catalytic nanomaterials

Jesús Muñiz · Enrique Sansores · Roger Castillo

Received: 1 December 2012 / Accepted: 11 May 2013 / Published online: 21 May 2013

Abstract The prediction of the series of $[Au_3X_3M_2]$ compounds (with X = H, F, Cl, Br, I and M = Li, Na, K, Rb, Cs) has been carried out by ab initio and DFT calculations. The systems are chemically stable due to their high chemical hardness. An unusual Au–Au attraction was found on each of the compounds along the series, addressing a strong metalophilic interaction of the aurophilic type. A strong aromatic character on the center of the $[Au_3X_3]^{2-}$ ring was also detected in the compounds under study, enhancing the stability of the species. The mechanism behind the bonding of the systems is mainly ruled by an electrostatic interaction among the 2 M^+ cations and the $[Au_3X_3]^{2-}$ monolayer sheet in accordance with CDA and Ziegler analysis; only a slight orbital contribution yielded by back-donation from the alkaline metals to the $[Au_3X_3]^{2-}$ monolayer sheet is involved. It was shown that the $[Au_3Cl_3M_2]$ group has the highest Fukui indexes, indicating that a catalytic reaction may rise from an electrophilic attack centered at the Au atoms or a nucleophilic attack on the alkaline-earth metals. The latter was tested with the most stable system of this group, namely $[Au_3Cl_3Li_2]$, allowing it to interact with a CO molecule; the optimized $[Au_3Cl_3Li_2]$ [CO] system represents a bound state that highlights the reactive properties of the species. An extended …–M–S–M–S–M–… (with S representing the $[Au_3X_3]^{2-}$ system) linear chain model was also predicted at DFT level. Considering its spatial representation of the frontier molecular orbitals, it was found that a possible electronic transfer along the chain may take place via the triggering of an electron, suggesting the existence of a nanowire.

Keywords Aurophilicity · ab initio calculations · Relativistic effects · Chemical reactivity · Aromaticity · Nanowire

1 Introduction

The theoretical and experimental study on metal monolayer sheets flanked by organic or inorganic ligands has been widely extended since the synthesis of ferrocene $[Fe(\eta^5C_5H_5)_2]$ [1] and has reached special attention from the discovery of sandwich Pd compounds $[Pd_3(C_7H_7)_2Cl_3]$ [PPh] and $[Pd_5(naphthacene)_2(toluene)][B(Ar_f)_4]_2(4\text{-toluene})]$, with $B(Ar_f)_4 = B[3,5(CF_3)_2C_6H_3]_4$ [2]. These kinds of complexes are important due to their several applications in catalysis, molecular recognition, polymers, optical and magnetic materials, nanodevices and medicine [1, 3]. For instance, the multidecker system $V_n(Bz)_{n+1}$ has been synthesized and theoretically studied, which is a ferromagnetic compound with unpaired electrons located on the metal atoms. This system is suggested to work as a building block material to be used on quantum computing and high-density information storage. Other sandwich complexes have also been theoretically studied [4] with organic or inorganic ligands, such as $BzMC_{60}$ (M = Sc-Co), and

Electronic supplementary material The online version of this article (doi:10.1007/s00214-013-1373-5) contains supplementary material, which is available to authorized users.

J. Muñiz (✉) · R. Castillo
Cuerpo Académico de Energía y Sustentabilidad, Universidad Politécnica de Chiapas, Calle Eduardo J. Selvas S/N, Col. Magisterial, C.P. 29082 Tuxtla, Chiapas, Mexico
e-mail: jmuniz@upchiapas.edu.mx

E. Sansores
Materia condensada y criogenia, Instituto de Investigaciones en Materiales, Universidad Nacional Autónoma de México, Apartado Postal 70-360, 04510 Mexico, DF, Mexico

experimentally synthesized [5] such as $Nd_2(COT'')_3$ (COT = η^8-cyclooctatetraenyl), a sandwich complex of three layers, that corresponds to the first linear homoleptic moiety.

Furthermore, some other studies have been carried out for Pd sandwich compounds: The characterization of the linear chain of Pd atoms flanked by organic materials, namely $[Pd_4(o\text{-}bpbb)_2][Bar^F]_2$, was synthesized by Tatsumi et al. [6]. The complex $[Pd_2([2.2]paracyclophane)_2(CH_3CN)_2][Bar^F_4]_2$ was also observed, which was characterized by Murahashi et al. [7], with a triangular tripalladium cluster at the central layer. Another example on tripalladium metal sheets is the series of sandwich complexes $[Pd_3Tr_2(E)_3][BF_4]_2$ (E = PPh_3, $AsPh_3$, and $SbPh_3$ and PEt_3) [8]. On the other hand, a square tetrapalladium sheet flanked by organic species was also synthesized by Murahashi et al. [9], that is, the complex $[Pd_4(\mu_4\text{-}C_9H9)(\mu_4\text{-}C_9H_9)][BAr_4]$. Scalar relativistic effects have also been considered in the study of sandwich complexes on the system $[(CNT)Pd_4(COT)]^{1+}$, where a σ-aromatic character was detected [10]. Some other inorganic sandwich complexes have been characterized, such as $[Ti(\eta^5P_5)_2]^{2-}$, which is a highly stable salt to heat and air, in solution and solid state [11]. Isoelectronic analogue systems of the latter have been theoretically predicted, that is, the systems $[Ti(\eta^5E_5)_2]^{2-}$ (E = CH, N, P, As, Sb). All complexes are prospective candidates in catalytic activity [2] as building blocks in larger systems where unsaturated hydrocarbons are adsorbed on metallic surfaces, giving them a use on the energy field [2], and they may also be combined as small discrete clusters with linker units to create an enhanced two-dimensional structure with modifiable structural and electronic properties, similar to those given by a one-dimensional molecular nanowire. Several theoretical efforts have been focused on the search of the existence and stability of sandwich monolayer sheet compounds with transition metal atoms at the extended Hückel level [12]. The ab initio and DFT predictions of the Au species $[Au_3Cl_3Tr_3]^{2+}$, a Au monolayer sheet capped by Cl atoms and flanked by two cycloheptatrienyl Tr^+ ligands, have been carried out by Muñiz et al. [13]. In this case, the bonding from the Tr ligands is ruled by a back-donation interaction to the bonding volume from the Au monolayer sheet to the Tr ligands. The mechanism behind the bonding in the $[Au_3Cl_3]^{2-}$ metal sheet is mainly ruled by a *d*–*d* orbital interaction mixed with a σ-character from the Au_{6s} orbitals. Particularly, Au–Au interactions were readily attributed to a closed-shell interaction, namely of the aurophilic type. Aurophilicity [14], a term initially given by Schmidbaur [15], is attributed to a shrinking on the Au–Au bonding distances, ranging from 300 to 360 pm. Exceptional cases with bond lengths shorter than 300 pm have also been observed [16]. The magnitude of the aurophilic attraction energy is of the order of the weakest covalent bonds and the strongest hydrogen bonds, an attraction energy ranging from 5 to 15 kcal/mol [17–20]. The origin of the interaction is mainly governed by relativistic and dispersion effects [16, 20]. The stability of the $[Au_3Cl_3Tr_2]^{2+}$ cluster was addressed to the aurophilic bonding present on the Au_3 central cluster and to the strong aromaticity reported on the compound [13]. The study was extended to the prediction of the $[Au_3Cl_3M_2]$ series, with M = Li, Na, K, Rb and Cs at MP2 (Moller–Plesset perturbation theory at second order) level [21]. Aurophilic effects were also involved in the attraction at the Au monolayer sheet, and a strong aromatic behavior was observed along the series, attributable to the *d*-electrons delocalization on the Au atoms of the monolayer sheet. Reactivity properties were also found in accordance with the Fukui scheme [22]. In this respect, it was known that Au has no reactive properties in bulk phase. Nevertheless, recent results reveal that, if Au is dispersed as fine particles on metal oxide surfaces, a wide range of oxidation reactions are accessed, especially the CO → CO_2 reaction [23, 24]. Regarding the energy field research, some theoretical studies have been achieved on the reactivity of Au clusters toward small molecules: It was found that the binding of methanol on positively charged clusters is stronger than that on neutral [25]. The combustion reaction of CO has been studied on a MgO-supported Au_8 cluster [26] and on a free anion dimer [27]. In the first instance, oxygen vacancies on the oxide surface play an important role on the catalytic activity of the cluster, and in the second, two reaction pathways were found for CO to CO_2 conversion. The presence of aromaticity has also been important in the electronic structure of metal clusters, since it has been shown to be present in coinage metal clusters [28, 29], reported at the DFT level of theory, that is, the complexes M_4H_4, with M = Cu, Ag, Au and a D_{4h} symmetry. M = Cu and Ag species present similar NICS values, and M = Au has the largest contribution. On the other hand, the series $[M_4Li_2]$ (M = Cu, Ag and Au) was also calculated at the DFT level, and a D_{4h} symmetry was also found in the series with a largest aromatic contribution coming from the M = Au species. It was shown that the aromatic characters in all these species are examples on *d*-aromaticity, where the contribution of the d_z^2 and d_{x-y}^{22} orbitals is behind it. Some other instances, such as $[M_4X]^-$ with X = Li and Na, were computed at the MP2 and CCSD(T) (couple cluster calculation with single and double substitutions with noniterative triple excitations) levels [30]. There is no systematic study performed on the chemical stability, catalytic properties, nor structural dependence of the bonding distance among alkaline ligands attached to Au atoms on clusters of the type $[Au_3X_3M_2]$, with X = H, Cl, I, F and M = Li, Na, K, Rb, Cs. Due to

the interesting electronic properties found in the previous study [21] for the $[Au_3Cl_3X_2]$ series of complexes (with X = Li, Na, K, Rb and Cs), the aim of this work is to generalize and to theoretically understand the bonding properties behind the $[Au_3X_3M_2]$ series of complexes, with M = Li, Na, K, Rb, Cs and X = H, Cl, I, F, study their chemical stability, locate reactive sites where catalytic activity may further take place and explore electronic transport properties.

2 Computational methods

Geometry optimizations were performed at the MP2 level of theory [31]. The methodology explicitly accounts with dispersion effects, which are essential to study the aurophilic attraction. We used the Stuttgart small-core pseudorelativistic effective core potential [32], defined with 19-valence electrons for the Au atoms. This pseudopotential was used with the valence triple-ζ plus one polarization type (TZVP basis set), calculated by Schäfer and optimized as a contracted Gaussian basis set [33]. Additionally, two f-type polarization functions, given by Pyykkö et al. [34], were augmented to the basis, namely $f = 0.2,\ 1.19$. The first function is a diffuse f orbital involved in the intermolecular interaction; the second one is a polarization function that describes the covalent bonding where the Au d^{10} shell is involved. The 6-31++G(2*df*, *p*) basis set was used for the Li, Na and K atoms; for the Rb and Cs atoms, the effective core potentials ECP28MDF and ECP46MDF were used with their corresponding basis sets. Such sets were optimized by the Stuttgart group [35], with the following contraction scheme: $(22s15p11d8f5g)/[14s11p9d8f5g]$ and $(27s19p13d10f5g)/[13s11p9d10f5g]$ for the Rb and Cs atoms, respectively. These are small-core 9-valence electron energy-consistent pseudopotentials that include scalar relativistic effects.

An energy decomposition analysis was performed to calculate the electrostatic and bonding energies in accordance with Ziegler's method [36, 37], which is defined for DFT. The methodology was carried out with the Slater's Xα exchange potential functional [38, 39], with $\alpha = 0.7$. It has been proven that this functional gives a good approximation to short-range interactions, such as the aurophilic attraction [40]. Besides, the Dirac methodology [41] was also used to calculate the atomic core orbitals that were kept unrelaxed on the complexes under study. The inner core shells were all fixed: For the Cl atoms, the shell $[1s^2–2p^6]$ was frozen, and $[1s^2]$, $[1s^2]$, $[1s^2–2p^6]$, $[1s^2–3d^2]$, $[1s^2–4d^{10}]$ and $[1s^2–4d^{10}]$ for Li, Na, K, Rb, Cs and Au, respectively. In all DFT calculations, the scalar relativistic zero-order relativistic approximation (ZORA) with spin–orbit effects was used, due to the important role that relativistic effects play in the aurophilic attraction [16]. In these calculations the Slater-type, high-quality triple-ζ plus one polarization basis set was used. Schleyer's nuclear independent chemical shift (NICS) method [42] was implemented to study the aromatic character in the series of complexes. The stability of the compounds was quantified through the chemical potential μ [43] and chemical hardness η [44]. These parameters were obtained from density functional theory as:

$$\mu = \left(\frac{\partial E}{\partial N}\right)_{T,v(r)} \tag{1}$$

and

$$\eta = \frac{1}{2}\left(\frac{\partial^2 E}{\partial N^2}\right)_{T,v(r)} \tag{2}$$

where E corresponds to the total energy, N is the total number of electrons, T is the temperature, and ν(r) is the external potential. In order to evaluate Eqs. (1) and (2), we applied a finite-difference approximation, assuming a quadratic-variation in E with respect to the number of electrons. That is, in orbital grounds, they may be written as:

$$\mu = -\left(\frac{IP + AE}{2}\right) \tag{3}$$

$$\eta = \left(\frac{IP - AE}{2}\right) \tag{4}$$

where IP stands for ionization potential and AE is the electron affinity. They can also be defined from Koopmans' theorem as $IP = -E_{\mathrm{HOMO}}$ and $AE = -E_{\mathrm{LUMO}}$, where E_{HOMO} corresponds to the energy of the highest occupied molecular orbital and E_{LUMO} to the energy of he lowest unoccupied molecular orbital. This approach has shown to give reliable results when aromatic and antiaromatic properties have been studied on metal systems in the context of the principles of maximum chemical hardness and minimum polarizability [45]. On the other hand, the atomic electronegativity in DFT methods is not so accurate since the first-row elements are not well described as the second-row elements, and this may be due to smaller size and larger effective nuclear charge and average internal potential. Furthermore, the density falls more rapidly, and it produces a higher density gradient. The above facts are not well described in the gradient corrected on the exact exchange functionals [46]. Taking the latter into account, the ab initio level of theory, namely the Hartree–Fock methodology, has been used to determine the chemical hardness [47, 48] and chemical potential [49] using Koopmans' theorem, which is exact in this context [50]. In order to study likely reactive sites in the title complexes, the Fukui local functions [50, 51] for electrophilic and nucleophilic agents were also

determined in a finite-difference ground through the gross natural charge (q) at site k (representing an atom in the molecule with $N-1$ and $N+1$ electrons). The Fukui index for electrophilic and nucleophilic attacks may be found from Eqs. (5) and (6), respectively.

$$f_k^- = q_k(N) - q_k(N-1) \tag{5}$$

and

$$f_k^+ = q_k(N+1) - q_k(N) \tag{6}$$

On the other hand, we also used local softness to compare reactivity properties among different species. Local softness is related to Fukui functions [50] through the equation

$$s(r) = \left(\frac{\partial\rho(r)}{\partial\mu}\right)_{v(r)} = \left(\frac{\partial\rho(r)}{\partial N}\right)_{v(r)}\left(\frac{\partial N}{\partial\mu}\right)_{v(r)} = f(r)S \tag{7}$$

where S is known as the global softness, defined as:

$$S = \frac{1}{2\eta} = \int s(r)\mathrm{d}r \tag{8}$$

Besides, as a consequence of the condition of normalization of the Fukui function, we have:

$$\int f(r)\mathrm{d}r = 1 \tag{9}$$

In this way, three different types of local softness related to the Fukui function are given by:

$$s^\alpha(r) = f^\alpha(r)S \tag{10}$$

The latter is defined for atomic properties in accordance with:

$$s_k^\alpha = f_k^\alpha S \tag{11}$$

Taking the latter into account, when two systems react, one of them will behave as a nucleophile or as an electrophile, depending on which has a higher or lower electrophilicity index, respectively. This global tendency comes from the local behavior of the molecules or from the atomic site where electrophilic or nucleophilic attack may take place. We used a generalized treatment as given by Chattaraj et al. [52], where the existence of a local electrophilicity index is considered, which changes from point to point in a molecule, and it is defined by:

$$\omega = \int \omega(r)\mathrm{d}r \tag{12}$$

Furthermore, it can also be represented using Eq. (9) as:

$$\omega(r) = \omega f(r) \tag{13}$$

We identify three different types of ω, called by Chattaraj et al. [52] *local philicity* indexes, since all different reactions are considered, namely:

$$\omega^\alpha(r) = \omega f^\alpha(r) \tag{14}$$

α may take the values $+$, $-$ and 0, corresponding to nucleophilic, electrophilic and radical attacks, respectively. It may also be defined for a specific atomic site k as

$$\omega_k^\alpha = \omega f_k^\alpha \tag{15}$$

which emphasizes the strength of the Fukui function and the frontier orbital theory [52].

The Herschbach–Lauri relation [20] was also used to estimate the aurophilic attraction:

$$R_{\mathrm{Au-Au}} = 268\ \mathrm{pm} + 29 \cdot \ln([\mathrm{N/cm}]/k_{\mathrm{Au-Au}}) \tag{16}$$

In Eq. (16), $R_{\mathrm{Au-Au}}$ is the equilibrium Au–Au distance and $k_{\mathrm{Au-Au}}$ is the force constant in N/cm. Interaction energies were also computed in accordance with Eq. (17):

$$V(R) = E_{\mathrm{AB}}^{\mathrm{AB}}(R) - E_{\mathrm{A}}^{\mathrm{AB}}(R) - E_{\mathrm{B}}^{\mathrm{AB}}(R) \tag{17}$$

where the lower index refers to the system under study, and the upper index to the basis set used. System A is the Au monolayer sheet $[Au_3X_3]^{-2}$ with X = H, Cl, F and I. System B corresponds to the 2 M^+ system, with M = Li, Na, K, Rb and Cs. Calculations were carried out using the computational code Gaussian 09 [53]. ZORA calculations were performed with the Amsterdam density functional (ADF) suite [54].

3 Results and discussion

3.1 Structural description

A series of $[Au_3X_3M_2]$ metal clusters, with X = H, F, Cl, I and M = Li, Na, K, Rb and Cs, have been predicted. All structures were optimized at the MP2 level of theory with the basis set described in the "Computational methods." Frequency calculations were also performed and no imaginary values were reported, indicating the presence of minima in all the series of compounds. Their molecular structures are depicted in Fig. 1, while their structural parameters are reported in Table 1. The $[Au_3X_3]^{-2}$ (with X = H,F, Cl and I) monolayer sheet is flanked by two M^+ cations (with M = Li, Na, K, Rb and Cs) with natural charges ranging from +0.915 to +0.991 (see Table S1 of Supplementary material), indicating that an ionic character is involved in the bonding.

The distance from the Au monolayer sheet to the M cations is symmetric at both sides of the Au_3 cluster and becomes longer as we interchange the M metal in the following order: Li < Na < K < Rb < Cs. On the other hand, the Au–X bonding distance is enlarged in the order H < F < Cl < I (see Table 1), which may be mainly attributed to the increase in the average distance from the

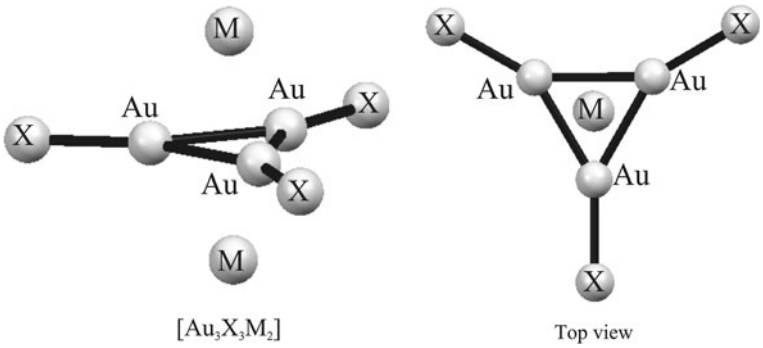

Fig. 1 Geometrical representation of the $[Au_3X_3M_2]$ series, with X = H, F, Cl, I and M = Li, Na, K, Rb, Cs (*left*). *Top view* of the system (*right*)

Table 1 Structural parameters of the series of $[Au_3X_3M_2]$ series, with X = H, F, Cl, I and M = Li, Na, K, Rb, Cs

MP2 computational method	$[Au_3H_3M_2]$				
Bond (pm)	$[Au_3H_3Li_2]$	$[Au_3H_3Na_2]$	$[Au_3H_3K_2]$	$[Au_3H_3Rb_2]$	$[Au_3H_3Cs_2]$
Au–Au	283.7 (293.4)	282.5 (293.0)	280.4 (288.4)	282.0 (288.1)	280.6 (287.2)
Au–H	160.6 (166.2)	161.4 (166.8)	168.0 (168.1)	162.5 (168.5)	162.7 (168.8)
Au_3–M	207.1 (197.4)	245.6 (248.5)	299.2 (305.1)	315.9 (326.6)	337.3 (342.8)
Point group	D_{3h}	D_{3h}	D_{3h}	D_{3h}	D_{3h}
ΔX_{MP2-HF}	9.7	10.5	8.0	6.1	6.6
Bond (pm)	$[Au_3F_3M_2]$				
	$[Au_3F_3Li_2]$	$[Au_3F_3Na_2]$	$[Au_3F_3K_2]$	$[Au_3F_3Rb_2]$	$[Au_3F_3Cs_2]$
Au–Au	273.8 (277.0)	273.0 (275.8)	273.2 (274.5)	272.3 (274.2)	272.0 (274.0)
Au–F	199.1 (200.4)	200.9 (202.0)	204.7 (203.4)	203.6 (204.0)	204.2 (204.5)
Au_3–M	215.5 (202.3)	254.4 (248.2)	305.4 (301.6)	325.0 (320.5)	346.4 (346.8)
Point group	D_{3h}	D_{3h}	D_{3h}	D_{3h}	D_{3h}
ΔX_{MP2-HF}	3.2	2.8	1.3	2.0	2.0
Bond (pm)	$[Au_3Cl_3M_2]$				
	$[Au_3Cl_3Li_2]$	$[Au_3Cl_3Na_2]$	$[Au_3Cl_3K_2]$	$[Au_3Cl_3Rb_2]$	$[Au_3Cl_3Cs_2]$
Au–Au	265.0 (279.0)	263.4 (277.7)	262.3 (276.1)	262.0 (276.0)	261.7 (275.6)
Au–Cl	230.4 (238.4)	232.0 (240.1)	233.7 (242.5)	234.0 (243.2)	234.5 (244.0)
Au_3–M	217.5 (220.1)	253.3 (261.3)	305.2 (322.8)	327.5 (338.7)	343.0 (360.3)
Point group	D_{3h}	D_{3h}	D_{3h}	D_{3h}	C_{3h}
ΔX_{MP2-HF}	14.0	14.3	13.8	14.0	13.9
Bond (pm)	$[Au_3I_3M_2]$				
	$[Au_3I_3Li_2]$	$[Au_3I_3Na_2]$	$[Au_3I_3K_2]$	$[Au_3I_3Rb_2]$	$[Au_3I_3Cs_2]$
Au–Au	266.8 (281.7)	265.2 (275.8)	264.1 (274.5)	263.6 (274.2)	263.4 (274.0)
Au–I	253.3 (265.7)	2.545 (201.9)	2.558 (203.4)	256.2 (204.0)	256.6 (204.5)
Au_3–M	216.7 (214.8)	259.2 (246.2)	309.0 (303.6)	324.8 (325.3)	344.6 (349.7)
Point group	D_{3h}	D_{3h}	D_{3h}	D_{3h}	D_{3h}
ΔX_{MP2-HF}	15.0	10.6	10.4	10.6	10.6

Values in parenthesis are HF results

valence electrons to the nucleus while going down the periodic table, consistent with the increasing principal quantum number of the valence region. Besides, the presence of the M^+ cations pushes away the X metal from the Au atom, increasing the Au–X distance in the following order: M = Li < Na < K < Rb < Cs. The latter may also be attributed to the increase in the electronic density given by the alkaline metals around the Au–X bonding distance

(see Fig. 1). The central Au_3 cluster presents an Au–Au bonding distance ranging from 281 to 284 pm for the $[Au_3H_3M_2]$ (with M = Li,Na, K, Rb and Cs) series. In the case of the $[Au_3F_3M_2]$ series, that distance ranges from 272 to 274 pm. On the other hand, the Au–Au bonding distance for the $[Au_3Cl_3M_2]$ series ranges from 261 to 265 pm and from 263 to 267 pm on the $[Au_3I_3M_2]$ series of compounds. In all the series of complexes, the Au–Au distance lies below the sum of the van der Waals radii ($\sim$300 pm), indicating the existence of the aurophilic attraction. Such an attraction may be attributed to dispersive effects [14, 16, 20], which have been explicitly included in the calculation by the MP2 methodology [31]. Full geometry optimizations have also been carried out at the Hartree–Fock (HF) level of theory, as presented in Table 1. The MP2 Au–Au bonding distances are contracted with respect to the SCF results. The difference between both methodologies may be attributed to dispersion effects, which are explicitly calculated in the MP2 methodology and are absent in the HF scheme. The bonding distance differences between MP2 and HF methodologies (ΔX_{MP2-HF}) are also presented in Table 1. On the $[Au_3H_3M_2]$ series, the ΔX_{MP2-HF} values reach a maximum at M = Na. ΔX_{MP2-HF} becomes constant for M = K, Rb and Cs. Due to the electronegativity of fluorine, the $[Au_3F_3M_2]$ series presents a different behavior, and the largest difference ΔX_{MP2-HF} is present in the $[Au_3F_3Li_2]$ complex. The latter highlights the importance of the dispersive attraction, which is the strongest along the series, since the ΔX_{MP2-HF} values are the largest. In particular, the $[Au_3F_3K_2]$ system has the highest value along this series. The rest of the ΔX_{MP2-HF} values remain constant for the rest of the species in this series.

The $[Au_3Cl_3M_2]$ and $[Au_3I_3M_2]$ series present the largest aurophilic attraction since the ΔX_{MP2-HF} bonding distance difference is largest with respect to the other series of complexes (14.0 and 11.4 pm in average for the $[Au_3Cl_3M_2]$ and $[Au_3I_3M_2]$ series, respectively). In order to quantify the aurophilic bonding, Au–Au Wiberg bond orders (Au_{WBO}) were computed for every series of complexes (see Table 2): In the $[Au_3X_3M_2]$ series, the Au_{WBO} indexes are the smallest, reaching a minimum at the $[Au_3X_3Rb_2]$ species.

The Au_{WBO} indexes for X = F,Cl and I are all about 0.43, addressing a larger overlap on the center of the ring and suggesting that the mechanism behind the aurophilic attraction, namely dispersion, may be strengthened by an orbital overlap. Nevertheless, dispersion interactions do not relate the rising of orbital overlap, since eventual covalent contributions may exist independently. This is also consistent with representative frontier molecular orbitals (MOs) depicted in Fig. 2: It is seen that they are mainly composed of Au_{6s} orbitals located at the metal monolayer sheet and significant d_{xz} and d_z^2 contributions located at the Au atoms on the ring. As it can be seen in Table S2, the natural charges reveal the breaking of the $5d^{10}$ shell and the partial filling of the 6*s* shell. This may be addressed to the large contribution of the Au_{6s} orbital, present on the frontier MOs HOMO-8, HOMO-10 and HOMO-11 on $[Au_3H_3Li_2]$, $[Au_3I_3Li_2]$ and $[Au_3F_3Li_2]$ compounds,

Table 2 Wiberg bond orders at the Au–Au bond in the $[Au_3X_3M_2]$ series, with X = H, F, Cl, I and M = Li, Na, K, Rb, Cs. NICS values and energy decomposition analysis in accordance with Ziegler's scheme

Complex	Li	Na	K	Rb	Cs
Wiberg bond orders (WBO)					
$[Au_3H_3M_2]$	0.34	0.38	0.38	0.41	0.40
$[Au_3F_3M_2]$	0.42	0.41	0.42	0.44	0.44
$[Au_3Cl_3M_2]$	0.40	0.43	0.44	0.46	0.46
$[Au_3I_3M_2]$	0.41	0.44	0.44	0.46	0.46
Nuclear independent chemical shift (NICS)					
$[Au_3H_3M_2]$	−32.5	−30.1	−30.5	−29.9	−30.3
$[Au_3F_3M_2]$	−48.5	−47.2	−46.4	−46.8	−46.9
$[Au_3Cl_3M_2]$	−38.3	−38.4	−39.0	−40.9	−39.3
$[Au_3I_3M_2]$	−31.1	−31.9	−32.9	−33.2	−33.5

Energy decomposition (kcal/mol)	ZORA			
	$[Au_3Cl_3Li_2]$	$[Au_3H_3Li_2]$	$[Au_3F_3Li_2]$	$[Au_3I_3Li_2]$
Pauli repulsion energy	+26.1	+38.3	+26.7	+26.7
Electrostatic attraction	−349.2	−408.2	−376.8	−335.8
Steric energy	−323.1	−370.0	−350.1	−309.3
Orbital relaxation	−72.0	−78.3	−61.0	−82.6
Total bonding energy	−395.1	−448.2	−411.1	−392.0

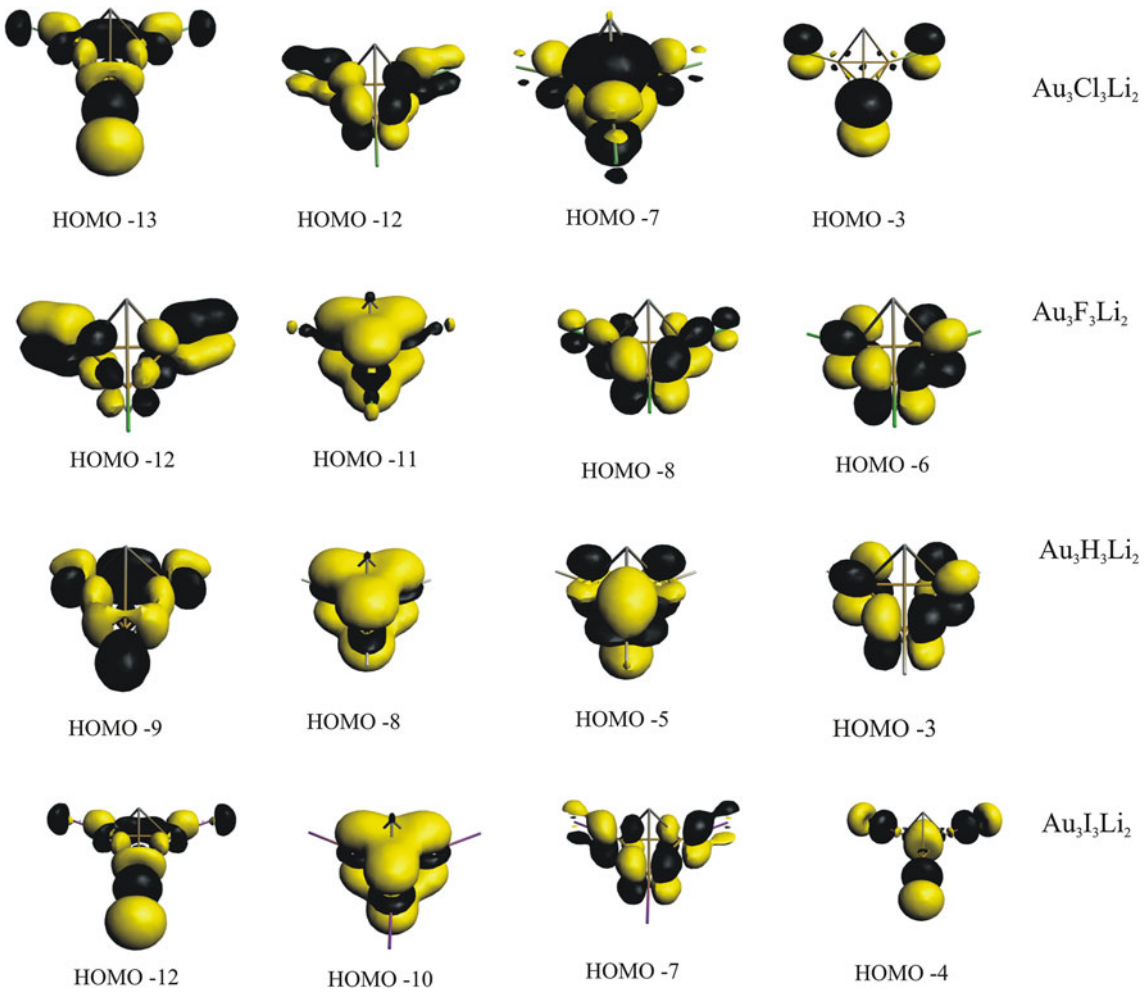

Fig. 2 Spatial distribution of frontier molecular orbitals at selected systems: $[Au_3Cl_3Li_2]$, $[Au_3F_3Li_2]$, $[Au_3X_3M_2]$, $[Au_3H_3Li_2]$ and $[Au_3I_3Li_2]$

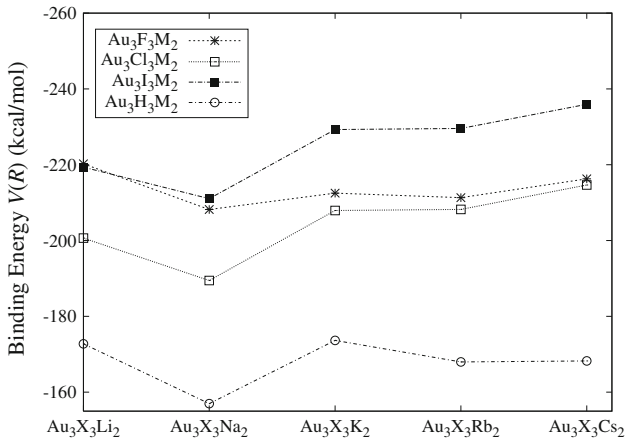

Fig. 3 Binding energies of the $[Au_3X_3M_2]$ series, with X = H, F, Cl, I and M = Li, Na, K, Rb, Cs

respectively. The rising of the d–d bonding observed on frontier MOs such as HOMO-3 and HOMO-6 on $[Au_3H_3Li_2]$ and $[Au_3F_3Li_2]$ systems is also involved.

Consequently, the dispersive effect that gives rise to the aurophilic bonding on the series of complexes is strengthened due to the 5*d*–6*s* electronic hybridization on the Au atoms at the monolayer sheet. Binding energies were also computed at the MP2 level in accordance with Eq. 17, and with the counterpoise method to account for the basis set superposition error.

As seen from Fig. 3, the compounds with the lowest binding energies in each group are presented in the following order: $[Au_3I_3Cs_2] < [Au_3F_3Li_2] < [Au_3Cl_3Cs_2] < [Au_3H_3K_2]$.

In these systems, the binding is more significant with heaviest M metal, that is, Cs. Nevertheless, in the case of X = F and H, lighter elements (M = Li and K, respectively) correspond to the largest binding energies of their groups.

The influence of the aurophilic effect on the bonding of the series of complexes was also verified using the Herschbach–Laurie relation (Eq. 16). It can also be compared with the MP2 Au–Au bonding distances. As it is reported

in Table 1, the Au–Au bonding distance ranges from 261.7 to 283.7 pm, while for the bonding distance predicted by Eq. 16, such values range from 252.6 to 280.0 pm (see Table S3 in the Supplementary material), indicating a reasonable agreement between both results.

3.2 Aromaticity

NICS values are presented in Table 2; as it can be seen, the $[Au_3F_3M_2]$ series of complexes presents the strongest aromatic character, ranging from −48.5 to −46.4 ppm in the following order for M: Li < Na < Cs < Rb < K. NICS values are also strong for the $[Au_3Cl_3M_2]$ series, with an average NICS value of −40 ppm. The isotropic currents, responsible for the strong aromatic character in the series of complexes, are generated at the center of the Au ring. They may rise from the electron delocalization at the frontier MO. As it is depicted in Fig. 2, the frontier MOs are mainly composed of d_z^2 and d_{xz} orbitals. Consequently, *d*-electrons may be the responsible for the strong aromatic character observed in the series of complexes, implying a δ-aromaticity, as it has previously been reported in analogous systems [28].

In order to test the scope of the Schleyer's methodology [42] to determine the aromaticity index in tridimensional molecules, NICS calculations were performed, considering the system with largest hardness, namely the $[Au_3Cl_3Li_2]$ cluster. As it is known, NICS criteria of aromaticity [42] are defined for planar, organic systems. It has been shown that the extension of such methodology can also be applied to tridimensional, sandwich metallic systems [10]. This assumption was tested by performing a NICS analysis with the $[Au_3Cl_3]$ and $[Au_3Cl_3Li_2]$ systems, for comparison. In this respect, a scanning of NICS values along the *z* coordinate for both clusters is presented in Fig. S1: It can be seen that for the $[Au_3Cl_3Li_2]$ system, the NICS (0) value reaches a maximum (see Fig. S1 in the Supplementary material) with −38.3 ppm at the center of the ring; in the analogue $[Au_3Cl_3Li_2]$ system, such value is decreased by 26 %, but still large with respect to organic complexes, such as benzene [42]. NICS values are symmetrically decreased as we move upward and downward the *z* axis along the geometrical center of the system and presumably due to the decrease in electron delocalization along the *z* axis. This behavior is conserved on the $[Au_3Cl_3Li_2]$ analogue, addressing a generality and validity on the use of the Schleyer's criteria of aromaticity for the tridimensional extended systems.

3.3 Chemical stability

Density functional theory and empirical observation dictate that there is a correlation between energetic stability and chemical hardness, that is, the greater the chemical hardness, the more stable the molecular system in a certain group of species. This statement has already been termed "the principle of maximum chemical hardness" [55–58]. Chemical hardness was evaluated in accordance with Eq. 4 from MP2 parameters since, as it was stated in the "Computational Methods," the ionization energies and electron affinities coming from ab initio results are more reliable than those that are obtained at the DFT level. In order to compute the chemical hardness as stated by Eq. 4, ionization potentials and electron affinities were obtained from Koopmans' theorem. As shown in Fig. 4, the chemical hardness along every $[Au_3X_3M_2]$ series of complexes presents a variation in the following order for M: Li > Na > K > Rb > Cs.

This indicates that the energetic stability is strengthened according to the size of the alkaline metal. Taking into account the increasing polarizability observed down the periodic table, it would appear that energy stabilization may be related to it. In this regard, polarizability computations were performed for the $[Au_3X_3M_2]$ series, with X = Cl, F, I, H and M = Li, Na, K, Rb, Cs (see Fig. S2 from the Supplementary material). An increasing behavior is reported only for the $[Au_3H_3M_2]$ and $[Au_3F_3M_2]$ series and an irregular behavior is reported for the $[Au_3Cl_3M_2]$ and $[Au_3I_3M_2]$ series, indicating that no evident correlation may be ascribed among chemical stability and polarizability. Light metals such as Li decrease considerably the hardness of the Au monolayer series $[Au_3X_3M_2]$, with X = Cl, F, I and H. This may be due to the electrostatic repulsion, which is larger along the series, and consequently, it destabilizes the compound decreasing the hardness (see Fig. 4). Furthermore, the chemical hardness presents a decreasing character along the series $[Au_3X_3M_2]$ in the following order for M: F > Cl > I > H. The latter

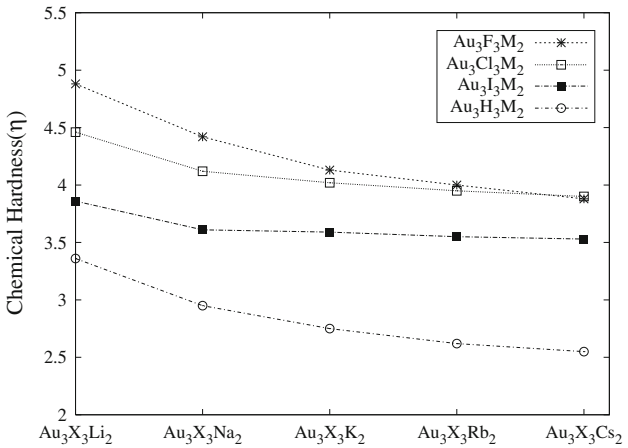

Fig. 4 Chemical hardness of the $[Au_3X_3M_2]$ series, with X = H, F, Cl, I and M = Li, Na, K, Rb, Cs

shows that the electronegativity is clearly related to the hardness, that is, the stronger the electronegativity, the larger the hardness. This behavior may be attributed to the enhanced electronegativity of the Au monolayer sheet coming from the X metal attached at the center of the ring. The values of chemical hardness given by the calculations give us insight into the stability of the series.

The parameters related to the normal mode of vibration for the $[Au_3Cl_3Li_2]$ system, such as frequency, molecular distortion in bond length and bond angles, are all presented in Table S4 in the Supplementary material. These parameters are reported to correlate them using a relationship between maximum hardness and minimum electrophilicity [59, 60]. It is known that the extremum on electrophilicity takes place at those points where the following equation holds:

$$\frac{\partial \mu}{\partial x} = \frac{\mu}{2\eta}\left(\frac{\partial \eta}{\partial x}\right) \tag{18}$$

where x represents any reaction coordinate. We have used x as bond length (stretching), bond angle (bending) and dihedral angle (internal rotation) into the system. Since $\mu < 0$, $\eta > 0$ due to convexity in energy. Consequently, extremum of electrophilicity takes place when the slopes of the variation in chemical potential and hardness present opposite signs.

Vibrational frequencies and chemical reactivity descriptors for $[Au_3Cl_3Li_2]$ complex are presented in Table S5 in the Supplementary material. The minimum energy–maximum chemical hardness is achieved for the ground-state structure. Nevertheless, the minimum polarizability criteria are not followed, since it corresponds to the ν14ls normal mode. On the other hand, the minimum electrophilicity corresponds to the ν17cas normal mode. It is known that minimum energy–minimum electrophilicity conditions are not held for all cases [59]. This may be addressed to the extremum condition that the constancy of the electrophilicity index is obtained when both μ and η are maximum or minimum or constant. The existence at the same time of both extremum conditions for chemical potential and hardness is not fulfilled for the $[Au_3Cl_3Li_2]$ complex at the ground-state geometry, and the condition of minimum energy–minimum electrophilicity does not apply. On the other hand, since distortions are within the permitted vibrational mode, the minimum energy–maximum hardness condition may be expected. Nevertheless, minimum electrophilicity–maximum hardness was not fulfilled due to changes in chemical hardness and chemical potential after distortion on the normal coordinates, consistent with the extremum conditions of electrophilicity.

In order to relate the aromatic behavior of the complexes under study with the stability and reactivity in the presence of the principles of maximum chemical hardness and minimum polarizability, we adopted the methodology given by Chattaraj et al. [45], where three aromaticity descriptors were defined: $\Delta X = X_{\text{cyclic}} - X_{\text{open}}$, with $X = E$, α and η. The cyclic systems where we applied the methodology were on the series $[Au_3Cl_3M_2]$ (M = Li, Na, K, Rb and Cs), due to the strongest aromaticity and highest chemical hardness reported among all species. Considering that the different electronic properties reported in this work are common through all the series, we can assume that the results given by the Chattaraj's analysis may be generalized for the rest of the series of complexes.

The parameters required to fulfill the corresponding open system values were computed from the planar isomer of $[Au_3Cl_3M_2]$ complex with M = Li, Na, K, Rb and Cs (see Fig. S3 in Supplementary material). According to the methodology, it is expected that an aromatic system posses negative ΔE and $\Delta\alpha$ values, but positive $\Delta\alpha$ values. The results for our calculations are reported in Table S6 of the Supplementary material; it can be observed that all values hold the condition given by Chattaraj, addressing a strong aromatic behavior, that is actually seen in this series of complexes given by NICS calculations.

3.4 Reactivity

The series of $[Au_3Cl_3M_2]$ complexes have shown to be prospective candidates to be used as catalysts [21], according to Fukui function calculations. This methodology is intended to study qualitatively the reactivity in molecular systems. We performed the calculations of the Fukui indexes of electrophilic attack (f^-) and nucleophilic attack (f^+), following the finite-difference approximation, as stated by Eqs. 5 and 6, respectively. The resulting indexes represent local parameters given by (f^-) and (f^+), providing insight into prospective sites in the system where reactivity may be important. All Fukui index calculations were performed using gross natural charges as stated in the computational methods. All calculations are reported from Figures S4 to S7 of Supplementary material. On the other hand, since it is desirable to compare the reactivity properties among complexes, the local softness (s) values are used. Such results are reported from Figures S8 to S11 from the Supplementary material.

It can be seen that the highest s^- local softness indexes correspond to the $[Au_3Cl_3M_2]$ and $[Au_3F_3M_2]$ series. In both cases, the Au_{s-} indexes increase in the order M = Li < Na < K < Rb < Cs ranging from +0.016 to +0.035. For comparison, the naked Au_3 cluster would have Au_{s-} index of about +0.16 for the neutral and cationic Au_3 cluster [21], after calculating the s^- index from the Fukui parameters. It is known that the naked Au_3 cluster presents reactivity properties that may be implemented in catalysis

applications [61]. Consequently, the series of compounds reported in this work present a reduced Au_{s-} index of local softness from that reported for the bare Au_3 cluster, indicating that a smaller probability of chemical reactivity, that is, an electrophilic attack, at the Au centers in the $[Au_3M_3X_2]$ compounds, may also arise. In this context, we studied the reactivity between two systems. As it is known [52], the Fukui function is an intramolecular index, not suitable to analyze intermolecular reactivity. In this respect, the local philicity $\omega_k^\alpha = \omega f_k^\alpha$ (with $\alpha = +, -, 0$, and k a given atomic site) is a more powerful parameter than the global electrophilicity, since the first contains the information of the second in addition to the site selectivity of the system toward electrophilic or nucleophilic attacks. Consequently, since the global electrophilicity of two different molecules is not the same, the best reactive sites of two different molecules for a given interaction can be understood only in the frame of local philicity and not on that of the Fukui function.

Particularly, the $[Au_3F_3M_2]$ and $[Au_3Cl_3M_2]$ species possess the highest Au_{s-} electrophilic indexes. The Au_{s-} values suggest that an acid-catalyzed reaction may take place at the Au sites in the $[Au_3X_3M_2]$ series with X = F and Cl. A direct application of this property [61] has been previously suggested: Environmental contaminant agents such as CO and NO may be absorbed by the cited species, since the MP2 natural charges of carbon and nitrogen are +0.616 and +0.318, respectively. According to the chemical hardness, the most stable species that may be appropriate candidates to be used as catalysts would be the species $[Au_3X_3M_2]$, with X = F and Cl and M = Na, K and Rb. Such complexes report the higher stability and larger electrophilic indexes. On the other hand, reactivity by protonation would be expected at the M cations due to their nucleophilic indexes ω_M^+ (ranging from +0.041 to +0.135) on virtually all species of the present work. Taking the latter into account, the calculations of local softness indexes indicate that a nucleophilic attack is likely to occur at the M cations. In order to test this conclusion, we perform a geometry optimization at the ZORA level between a CO molecule and the system $[Au_3Cl_3Li_2]$ (which has been shown to be one of the most stable species in this work) to study the resulting interaction. The system $[Au_3Cl_3Li_2][CO]$ was readily obtained (see Fig. 5). In this respect, the carbon monoxide system is a contaminant agent, common in several combustion processes [26, 27], that is desirable to be depleted when it is released into the environment. We propose the species $[Au_3Cl_3Li_2]$ due to its high stability given by the chemical hardness to interact with a CO molecule at the scalar relativistic ZORA level. No stable configurations were found where the CO molecule is adsorbed by $[Au_3Cl_3Li_2]$ catalyst at the Au sites. Nevertheless, a minimum was found where the CO

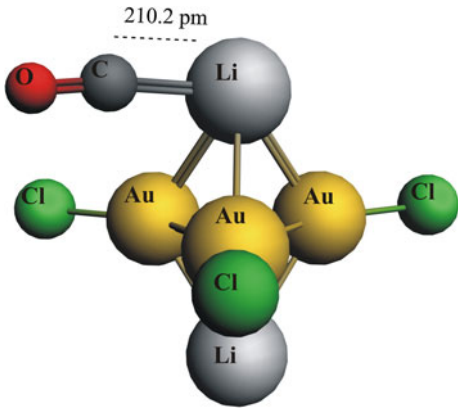

Fig. 5 Ground-state geometry of the system $[Au_3Cl_3Li_2][CO]$

interacts directly with a Li center, with a bonding distance of 210.2 pm (see Fig. 5). The Au–Au bonding distances remain virtually unaltered, while the Au_3–M distance shrinks 10 pm from the original MP2 optimized parameter (Table 1). Consequently, the species would be structurally unaltered due to its high stability, and the Au system, acting as a catalyst, would be recovered after an absorption process. This indicates that a base-catalyzed reaction would be expected and would be more favorable than an acid-catalyzed reaction at the Au centers.

3.5 Energy decomposition analysis

In order to have a wider picture on the interactions involved in the bonding nature, a charge decomposition analysis (CDA) was carried out. The CDA scheme partitions a system into two fragments to give a deeper understanding on the donor–acceptor interactions. The wave functions of the compound are built to define a linear combination of donor and acceptor fragment orbitals (LCFO). The CDA scheme evaluates the donated charge from the occupied orbitals of the donors to the unoccupied orbitals of the acceptor. On the other hand, the methodology also evaluates the contribution coming from a back-donation from the occupied orbitals of the acceptor to the unoccupied orbitals of the donor. The CDA scheme also computes the repulsive polarization, giving the charge depleted from the overlapping region of the occupied orbitals of the acceptor and donor fragments. As it can be seen from Figures S12 to S15, the donation contribution in all complexes of the series is virtually absent, due to the negative values depicted in the figures. Consequently, no electronic charge is transferred to the bonding volume. As depicted from Fig. S12 to S15 in the Supplementary material, a slight back-donation contribution coming from the fragment monolayer sheet $[Au_3X_3]^{2-}$ (with X = H, Cl, I and F) to the alkaline metal M^+ with M = Li, Na, K, Rb and Cs is observed in all species of the series. The repulsive polarization interaction

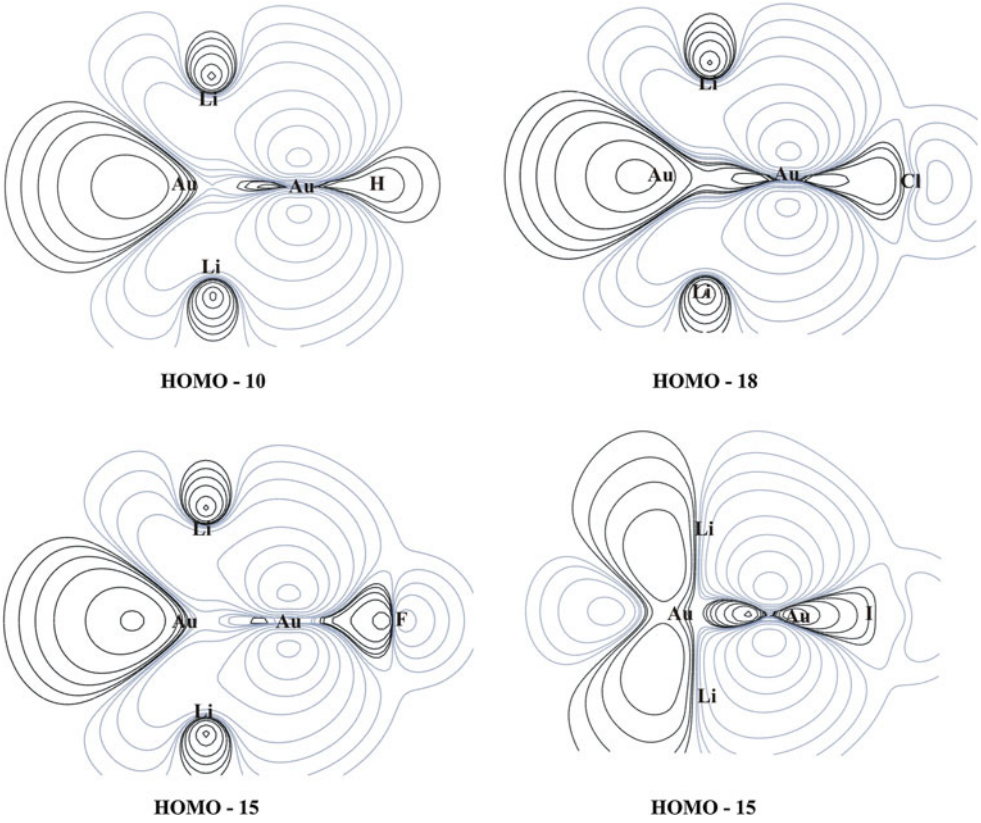

Fig. 6 Lateral view of selected frontier MO of $[Au_3H_3Li_2]$, $[Au_3Cl_3Li_2]$, $[Au_3F_3Li_2]$ and $[Au_3I_3Li_2]$

is negligible, since negative values are reported in all cases, and does not constitute part of the bonding structure. Figure 6 shows a perpendicular contour to the plane of the Au_3 monolayer sheet of the molecular orbitals mainly involved in the back-donation interactions. As it can be seen on the slices, the electronic charge is mainly located near the plane of the metal sheet, and it is related to the strong contribution coming from the *d*-electrons on the Au atoms, which are also involved in the δ-aromaticity described in a former section.

Energy-correlation diagrams are reported in order to understand the mechanism of bonding on the most stable systems of each series. According to chemical hardness, those systems are $[Au_3X_3Li_2]$ with X = H, Cl, F and I. The analysis was performed by partitioning the complex into two fragments: $[Au_3X_3]^{2-}$ and M^+ ions. The main orbital contributions involved in the bonding from both fragments are depicted in Figure S16, for the $[Au_3Cl_3Li_2]$ complex. In this case, the $[Au_3Cl_3]$ fragment contributes to the bonding with d_z^2 and d_{xz} orbitals, located at the Au_3 clusters, and also with *p*-orbitals allocated at the Cl atoms. The Li_2 fragment contributes to the bonding with a σ orbital at the HOMO. The resulting MOs involved in the bonding are shown in Fig. 2. As it can be seen, all MOs from the $[Au_3Cl_3]$ fragment appear on the MOs of the total $[Au_3Cl_3Li_2]$ complex. Only a contribution coming from the HOMO of the Li_2 fragment is present at the HOMO-11 of the $[Au_3Cl_3Li_2]$ compound. Consequently, the bonding may be mainly addressed to an electrostatic interaction.

In the case of the $[Au_3H_3Li_2]$ system (see Figure S17), the HOMO-5 of $[Au_3H_3]^{-2}$ fragment has a σ–σ* orbital interaction, located at the center of the Au_3 ring. A contribution from d_{xz} orbitals allocated at the HOMO-1 and HOMO-3 is also important.

The Li_2 fragment also contributes with the s bonding orbital described on the latter system and interacts with the doubly degenerate HOMO-5 of the $[Au_3H_3]^{-2}$ fragment, giving rise to the bonding HOMO-8 on the $[Au_3H_3Li_2]$ complex (see Fig. 2). The $[Au_3H_3]^{-2}$ HOMO-5 is basically the same as 6*s* bonding $[Au_3H_3Li_2]$ HOMO-8. The same behavior is depicted in Figures S18 and S19 for the $[Au_3F_3Li_2]$ and $[Au_3I_3Li_2]$ systems, respectively, where the bonding orbitals are mainly formed by *d*-orbitals on the $[Au_3X_3]^{-2}$ clusters, with X = F and I. In order to quantify the contributions from the bonding energy involved in the interaction between the most stable systems, we performed an energy decomposition analysis using the Ziegler's methodology [36, 37] at the ZORA DFT/Xα//MP2 level of theory [31, 38]. On this scheme, the total interaction energy is divided into three parts: (1) the Pauli repulsion energy (E_{Pauli}), (2) the orbital interaction and (3) the electrostatic attraction (E_{Elec}). E_{Pauli} corresponds to an increase in the kinetic energy of the electrons in the system as stated by the Pauli principle.

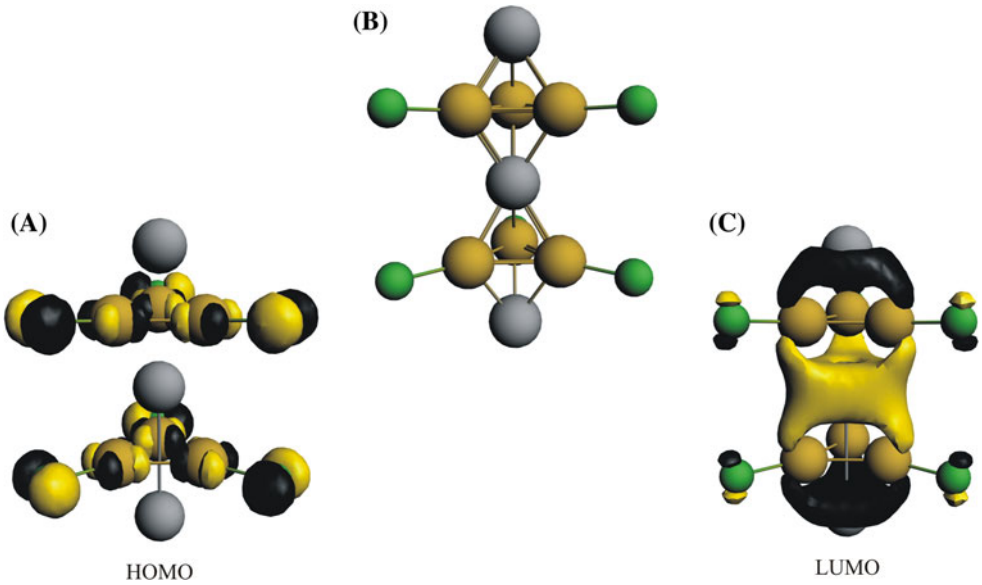

Fig. 7 …M–S–M–S–M–… linear chain model. **a** Spatial representation of the HOMO, **b** ground-state geometry of the model, **c** spatial representation of the LUMO

The third contribution is the attractive electrostatic overlap interaction (E_{Elec}). The steric energy contribution comes from adding up E_{Pauli} and E_{Elec}. On Ziegler's scheme, the $[Au_3X_3]^{-2}$ metal sheet and the 2 M^+ cations are taken into account as individual fragments in order to compute the Pauli repulsion and electrostatic interaction; their corresponding MOs remain fixed. When the occupied and virtual MOs of $[Au_3X_3]^{-2}$ and 2 M^+ fragments are mixed, we obtain the orbital relaxation energy. The polarization term and charge transfer are relevant in this contribution due to the electronic population that gives rise to the charge transfer. The former comes from the occupied orbitals of the first fragment to the unoccupied orbitals of the second one. Furthermore, the polarization contribution originates in the charge transfer from the occupied orbitals of a particular fragment to its own unoccupied orbitals. The energy decomposition as given by Ziegler's methodology [36, 37] is presented in Table 2. The results suggest that the electrostatic attraction is the main contribution to the total bonding energy of the most stable complexes of the series. That is, the electrostatic energy is the main term on the energy decomposition in the order $[Au_3H_3Li_2] > [Au_3F_3Li_2] > [Au_3Cl_3Li_2] > [Au_3I_3Li_2]$, representing 82, 92, 88 and 86 % of their corresponding total bonding energy. This is consistent with the initial charges of species $[Au_3X_3]^{2-}$ and the M^+ ions. This is also in agreement with the CDA analysis presented before, and it may be extended to all species in the title complexes.

3.6 Further possible electronic transfer mechanisms

A possible generalization of the compounds under study would be an infinite, one-dimensional chain …–M–S–M–S–…, where S represents the $[Au_3X_3]$ group and M a divalent metal atom, given by the alkaline earth. Due to the high stability of the $[Au_3Cl_3Li_2]$ system, we propose a simplified model of the one-dimensional chain that would form such a structure. A ZORA optimization was performed, and a ground state was found with no imaginary frequencies (see Fig. 19). The Au–Au bonding distance is contracted 1.6 pm with respect to that of a single $[Au_3Cl_3Li_2]$ unit, strengthening the aurophilic interaction, while the Au_3–M distance is also contracted by 5.3 pm, giving stability to this nanostructure. The optimized model suggests that an infinite polymer may be build with the $[Au_3Cl_3Li_2]$ species, as the building block. The spatial representation of the HOMO and LUMO is shown in Fig. 7: The HOMO allocates d-electrons on the Au atoms that may be transferred from each $[Au_3Cl_3Li_2]$ unit to the other, since the LUMO is mainly allocated on the Li atom that connects every monolayer metal sheet. Furthermore, a linear current may be triggered along the –M–S–M–S– chain structure, giving rise to the origin of a nanowire.

4 Conclusions

The prediction of the series of complexes $[Au_3X_3M_2]$ with X = H, F, Cl, I and M = Li, Cl, Na, K, Rb, Cs was carried out for the first time. The stability on the series was tested in accordance with the chemical hardness criteria, indicating that the compounds $[Au_3X_3M_2]$ with X = H, F, Cl, I and M = Li are the most stable of each corresponding series. NICS calculations reveal a strong aromaticity in every species of the series, making evident the stability of the compounds. The aromaticity of the series is mainly ruled by a large contribution coming from the d-orbitals located at the frontier MOs on the center of the Au_3

monolayer sheet; consequently, a δ-aromaticity would be expected. A correlation between the chemical hardness and NICS values was also found, indicating that while the NICS values become larger, the species under study become more chemically stable. Besides, the aromaticity descriptors suggested in this work are consistent with the criteria of aromaticity given by energetics and NICS values through magnetic character. Fukui indexes indicate that the systems under study are highly reactive at the Au sites with an electrophilic attack and are reactive at the alkaline metal M = Li, Na, K, Rb and Cs as a nucleophilic attack, which was already tested with a CO molecule where the $[Au_3Cl_3Li_2]$ acted as a catalyst. CDA analysis reveals that the bonding nature of all the species comes from slight back-donation contributions and is mainly ruled by an electrostatic attraction. The series of complexes are promising candidates to be used as nanowires forming a one-dimensional chain, due to a favorable electronic transport mediated by the frontier molecular orbitals.

Acknowledgments J.M. wants to acknowledge Consejo Nacional de Ciencia y Tecnología (CONACYT-México) for financial support under Grant No. 156591, Programa de Mejoramiento del Profesorado (PROMEP-SEP) under Grant No. UPCHS-PTC-039 and Itzel Flores and Constanza Muñiz for technical support. E.S. would like to also acknowledge DGCTIC and the Supercomputing Department of the Universidad Nacional Autónoma de México for the computing resources. The study was dedicated to the memory of Porfirio Soria Guzmán (1934–2012).

References

1. Wilkinson G, Rosenblum M, Whiting MC, Woodward RB (1952) J Am Chem Soc 74:2125–2126
2. Murahashi T, Fujimoto T, Oka M, Hashimoto Y, Uemura T, Tatsumi Y, Nakao Y, Ikeda A, Sakaki S, Kurosawa H (2006) Science 313:1104–1107
3. Muetterties EL, Bleeke JR, Wucherer EJ, Albright TA (1982) Chem Rev 82:499–525
4. Zhu L, Zhang T, Yi M, Wang J (2010) J Phys Chem A 114:9398–9403
5. Lorenz V, Hrib SBCG, Edelmann FT (2010) Organometallics 29:4787–4789
6. Tatsumi Y, Shirato K, Murahashi T, Ogoshi S, Kurosawa S (2006) Angew Chem Int Ed 45:5799–5803
7. Murahashi T, Fujimoto M, Kawabata Y, Inoue R, Ogoshi S, Kurosawa H (2007) Angew Chem Int Ed 46:5440–5443
8. Babbini DC, Mulligan FL, Schulhauser HR, Sweigart TC, Nichol GS, Hurst SK (2010) Inorg Chem 49:4307–4312
9. Murahashi T, Inoue R, Usui K, Ogoshi S (2009) J Am Chem Soc 131:9888–9889
10. Muñoz-Castro A, Carey DM-L, Arratia-Pérez RJ (2010) J Chem Phys 132:164308–164314
11. Urnezius E, Brennessel WW, Cramer CJ, Ellis JE, von Schleyer PR (2002) Science 295:832–834
12. Burdett JK, Canadell E (1985) Organometallics 4:805–815
13. Muñiz J, Sansores LE, Martínez A, Salcedo R (2008) J Mol Model 14:417–425
14. Muñiz J, Wang C, Pyykkö P (2011) Chem Eur J 17:368–377
15. Schmidbaur H (1990) Gold Bull 23:11–21
16. Pyykkö P (2004) Angew Chem Int Ed 43:4412–4456
17. Schmidbaur H (1995) Chem Soc Rev 24:391–400
18. Mingos DMP (1996) J Chem Soc Dalton Trans 5:561–566
19. van Zyl WE, de Luzuriaga JML, Fackler JPJ (2000) J Mol Struct 516:99–106
20. Pyykkö P (1997) Chem Rev 97:597–636
21. Muñiz J, Sansores LE, Pyykkö P, Martínez A, Salcedo R (2009) J Mol Model 15:1165–1173
22. Yang W, Mortier WJ (1986) J Am Chem Soc 108:5708–5711
23. Valden M, Lai X, Goodman DW (1998) Science 281:1647–1650
24. Grunwaldt JD, Baiker A (1999) J Phys Chem B 103:1002–1012
25. Rousseau R, Marx D (2000) J Chem Phys 112:761–769
26. Sánchez A, Abbet S, Heiz U, Schneider W-D, Häkkinen H, Barnett RN, Landman U (1999) J Phys Chem A 103:9573–9578
27. Häkkinen H, Landman U (2001) J Am Chem Soc 123:9704–9705
28. Tsipis AC, Tsipis CA (2003) J Am Chem Soc 125:1136–1137
29. Tsipis CA, Karagiannis EE, Kladou PF, Tsipis AC (2004) J Am Chem Soc 126:12916–12929
30. Lin Y-C, Sundholm D, Jusélius J, Cui L-F, Li X, Zhai H-J, Wang L-S (2006) J Phys Chem A 110:4244–4250
31. Møller C, Plesset MS (1934) Phys Rev 46:618–622
32. Andrae D, Häussermann U, Dolg M, Stoll H, Preuss H (1990) Theor Chim Acta 77:123–141
33. Schäfer A, Huber C, Ahlrichs R (1994) J Chem Phys 100:5829–5835
34. Pyykkö P, Runeberg N, Mendizabal F (1997) Chem Eur J 3:1451–1457
35. Lim IS, Schwerdtfeger P, Metz B, Stoll H (2005) J Chem Phys 122:104103–104115
36. Ziegler T, Rauk A (1977) Theor Chim Acta 46:1–10
37. Ziegler T, Rauk A, Baerends EJ (1977) Theor Chim Acta 43:261–271
38. Slater JC (1951) Phys Rev 81:385–390
39. Schwarz K (1972) Phys Rev B 5:2466–2468
40. Wang S-G, Schwarz WHE (2004) J Am Chem Soc 126:1266–1276
41. Velde GT, Bickelhaupt FM, Baerends EJ, Guerra CF, Gisbergen SJAV, Snijders JG, Ziegler TJ (2001) Comput Chem 22:931–967
42. von Schleyer PR, Maerker C, Dransfeld A, Jiao H, van Eikema Hommes NJR (1996) J Am Chem Soc 118:6317–6318
43. Ghosh SK, Berkowitz M (1985) J Chem Phys 83:2976–2983
44. Berkowitz M, Ghosh SK, Parr RG (1985) J Am Chem Soc 107:6811–6814
45. Chattaraj P, Roy D, Elango M, Subramanian V (2005) J Phys Chem A 109:9590–9597
46. Kanakaraju R, Kolandaivel P, Gowenlock B (2002) J Mol Struct (Theochem) 577:121–129
47. Lewars E (2003) Computational chemistry. Kluwer Academic Publishers, Massachusetts
48. Koopmans T (1934) Physica 1:104–113
49. Szabo A, Ostlund N (1989) Modern quantum chemistry. Dover Publication, Inc., New York
50. Parr RG, Yang W (1989) Density-functional theory of atoms and molecules. Oxford Science Publications, New York
51. Parr RG, Yang W (1984) J Am Chem Soc 106:4049–4050
52. Chattaraj PK, Maiti B, Sarkar U (2003) J Phys Chem A 107:4973–4975
53. Frisch MJ, Trucks GW, Schlegel HB, Scuseria GE, Robb MA, Cheeseman JR, Scalmani G, Barone V, Mennucci B, Petersson GA, Nakatsuji H, Caricato M, Li X, Hratchian HP, Izmaylov AF, Bloino J, Zheng G, Sonnenberg JL, Hada M, Ehara M, Toyota K, Fukuda R, Hasegawa J, Ishida M, Nakajima T, Honda Y, Kitao O, Nakai H, Vreven T, Jr. JAM, Peralta JE, Ogliaro F, Bearpark M, Heyd JJ, Brothers E, Kudin KN, Staroverov VN, Kobayashi

R, Normand J, Raghavachari K, Rendell A, Burant JC, Iyengar SS, Tomasi J, Cossi M, Rega N, Millam JM, Klene M, Knox JE, Cross JB, Bakken V, Adamo C, Jaramillo J, Gomperts R, Stratmann RE, Yazyev O, Austin AJ, Cammi R, Pomelli C, Ochterski JW, Martin RL, Morokuma K, Zakrzewski VG, Voth GA, Salvador P, Dannenberg JJ, Dapprich S, Daniels AD, Farkas O, Foresman JB, Ortiz JV, Cioslowski J, Fox DJ (2009) Gaussian 09 revision B.01. Gaussian Inc., Wallingford CT

54. Baerends EJ, Autschbach J, Bérces A, Bo C, Boerrigter PM, Cavallo L, Chong DP, Deng L, Dickson RM, Ellis DE, Fan L, Fischer TH, Fonseca-Guerra C, van Gisbergen SJA, Groeneveld JA, Gritsenko OV, Grüning M, Harris FE, van den Hoek P, Jacobsen H, van Kessel G, Kootstra F, van Lenthe E, Osinga VP, Patchkovskii S, Philipsen PHT, Post D, Pye CC, Ravenek W, Ros P, Schipper PRT, Schreckenbach G, Snijders JG, Sola M, Swart M, Swerhone D, te Velde G, Vernooijs P, Versluis L, Visser O, van Wezenbeek E, Wiesenekker G, Wolff SK, Woo TK, Ziegler T. Amsterdam density functional (ADF), theoretical chemistry. Vrije Universiteit, Amsterdam http://www.scm.com
55. Parr RG, Pearson RG (1983) J Am Chem Soc 105:7512–7516
56. Pearson RG (1987) J Chem Educ 64:561–567
57. Parr RG, Chattaraj PK (1991) J Am Chem Soc 113:1854–1855
58. Parr RG, Gázquez JL (1993) J Phys Chem 97:3939–3940
59. Parthasarathi R, Elango M, Subramanian V, Chattaraj PK (2005) Theor Chem Acc 113:257–266
60. Chamorro E, Chattaraj PK, Fuentealba P (2003) J Phys Chem A 107:7068–7072
61. Wu X, Senapati L, Nayak SK, Selloni A, Hajaligol M (2002) J Chem Phys 117:4010–4015